Parameterizing subgrid scale eddy effects in a shallow water model

Eugene Kazantsev

Parameterizing subgrid scale eddy effects in a shallow water model

Eugene Kazantsev
INRIA, projet AirSea, Laboratoire Jean Kuntzmann, 700, avenue Centrale 38400, Saint Martin d'Hères, France. E-mail: kazan@imag.fr

Abstract

Basing on the maximum entropy production principle, the influence of subgrid scales on the flow is presented as the harmonic dissipation accompanied by the backscattering of the dissipated energy. This parametrization is tested on the shallow water model in a square box. The closure problem is analyzed basing on the balance between the dissipation of energy and its backscattering. Results of this model on the coarse resolution grid are compared with the reference simulation at four times higher resolution. It is shown that the mean flow is correctly recovered, as well as variability properties, such as eddy kinetic energy fields and its spectrum.

keywords: Subgrid scales; Backscattering; Shallow water, Viscous flow; Turbulent flow.

1 Introduction

The necessity to discretize the model equations on finite-resolution spatial and temporal grids implies the existence of subgrid processes, i.e. those which are not resolved by the grid and thus excluded from any explicit simulation. Among such processes one can cite the molecular diffusion and viscosity, three-dimensional turbulence, convection and the unresolved portion of the spectrum of mesoscale turbulent eddies.

The earliest attempts to include some of the effects of smaller-scale processes on the larger scales date back to Boussinesq and Reynolds. Boussinesq [1] formed hypothesis that exists some analogy between molecular and turbulent viscosity. He claimed that, analogically to the Newton's law, it is possible to express turbulent stress in similar way as shear stress.

Reynolds [2] decomposed hydrodynamic variables into large-scale and smaller-scale components supposing that these scales are clearly separated in spectral space. Analyzing the influence of small-scale processes, he derived the Reynolds

stress tensor composed by correlations of small-scale variables representing the mean turbulent momentum fluxes and shearing stresses.

Dealing with the Reynolds stress tensor, we get a so-called closure problem. System cannot be closed directly by equations for Reynolds stresses because equations contain higher order correlations. Using the Boussinesq hypothesis, we can introduce the turbulent (or eddy) viscosity and approximate the Reynolds stress tensor by means of the large-scale variables. Despite great differences between molecular and turbulent viscosity, Boussinesq closure gives satisfying results in prediction of simple flows.

Accurate simulation of more complex flows at higher resolutions requires a finer parametrization of subgrid scale eddies, that's why the eddy-viscosity turbulence models are the subject of thousands of papers in the XXth century. It is absolutely impossible to cite even the most important of them. However, overwhelming majority of these papers discuss various formulations of the dissipation operator without any energetically positive impact to large scale flow. Indeed, the dissipation must be the principal influence of small scales. Analyzing quasi-geostrophic turbulence, Charney [3] has shown that its fundamental property is the transfer of enstrophy to smaller and smaller scales by non-linear advection. Enstrophy, consequently must be removed near the grid scales simulating a net transfer to subgrid scales in order to avoid accumulation.

However, if the model resolution is sufficiently fine, a parametrization of eddy-viscosity dissipates not only enstrophy, but also a part of kinetic energy. This energy transfer may be considered as undesirable or spurious because it results in too little grid-scale eddy kinetic energy and too weak eddy induced transport.

The idea of possible negative eddy viscosity was introduced by Kraichan in [4], who studied two- and three-dimensional turbulence at large and small scales. Leith [5] introduced the stochastic backscatter term to simulate the subgrid scales contribution to the energy balance by injecting noise into the system. Another stochastic backscatter forcing was proposed in [6] and tested in frames of ensemble forecasting by the ECMWF model.

Other promising approaches to avoid energy dissipation by sub-grid scales have been discussed during last 20 years. So far, it is only possible to parametrize the statistical effects of the subgrid eddies, statistical closure theory seems to be a natural formulation for developing self-consistent subgrid models. Thus, requirements of the energy conservation and the maximum entropy production has been used in [7] to simulate the influence of subgrid scales in the barotropic vorticity equation. It has been shown that the mean flow is correctly recovered, as well as the variability properties, such as the kinetic energy fields and the eddy flux of potential vorticity compared with the reference simulations at a resolution four times higher. However, generalization of this approach to shallow water and primitive equations models faced some difficulties [8, 9].

Another interesting approach that must be mentioned is the alpha-model approach [10]. Alpha model arises from a Lagrangian averaging of NavierStokes equations [11]. It includes a modification of the nonlinear advection and can be considered as a regularization approach to modelling turbulence. The alpha

model has been used to simulate the barotropic flow forced by double gyre wind stress [12]. The results show that the alpha term leads to more realistic gyre structures and smoother solutions at coarse resolution with lower value of viscosity. However, in some cases, the alpha sub-grid term may cause a forward transfer of energy and enstrophy at scales larger than the filter scale leading to the accumulation of enstrophy at small scales [13].

An idea to use an explicit forcing that simulates the energy flux from small scales intended to compensate the spurious energy dissipation, while maintaining dissipation of enstrophy has been expressed in [14]. Two kind of such forcings (also called backscatter term) has been discussed. One of them represent an uncorrelated Gaussian noise and another one use a negative Laplacian viscosity (while the general positive dissipation is assured by a bilaplacian). This idea was further developed in [15] by implementation in a primitive-equation model and by the formulation of a new prognostic variable that accounts for the sub-grid budget of the eddy kinetic energy, allowing to better represent spatial inhomogeneities in the eddy field. These backscatter forcings are tested in frames of two-layer quasi-geostrophic model [14] and in an idealized configurations of a primitive equation ocean model [15], and are shown to improve the simulations at typical eddy-permitting resolutions.

However, it is quite difficult to understand either physical or numerical basis of these compensative backscatters. No physical background is presented to advocate either stochastic or deterministic energy backscatter. The approach can only be used with the biharmonic dissipation while numerous models with insufficient resolution use a Laplacian.

In this paper we generalize the approach described in [7] to be used in primitive equations ocean models. The approach was tested in frames of barotropic divergenceless flow. However, in real world applications we have to work with more complex flows. Primitive equations represent now the basis of the majority of global ocean models and a great part of regional ones. That's why the main goal of our efforts will be focused on these equations.

The main idea expressed in [7] is based on the supposition that potential vorticity may have a fine, subgrid-scale structure while streamfunction is supposed to be smooth. That means we suppose that only vorticity has considerable variations within a grid cell. These variations are described by a probability density function that determines the entropy. Together with the maximization of the entropy production, we require strict conservation of the kinetic energy also. In frames of barotropic vorticity equation, there is no ambiguity in choice of these two variables.

Generalization of this approach to more complex model leads to such an ambiguity. Even working with a shallow water model we must choose either potential or relative vorticity to have a subgrid scale variations and either kinetic or total energy to be conserved. Moreover, shallow water flow is not completely divergenceless. It has been supposed in [8] that divergence in shallow water model can be neglected in front of potential vorticity. But, this hypothesis results in no divergence dissipation at grid scales and leads to numerical instability. Consequently, we have to include the divergence in the list of variables

having a subgrid structure.

The choice of potential vorticity as a principal variable having the subgrid variations in frames of barotropic or shallow water models may be motivated by the fact that potential vorticity in these models is simply transported by advection. Hence, we may suppose that its subgrid-scale patches are also transported and conserved by the explicit velocity field. However, if we add the divergence to the list of variables having a subgrid structure, this advantage can no longer be used: no form of the divergence can be considered as transported. Moreover, even low but non-null divergence mixes subgrid vorticity patches and we can no longer suppose that they are transported.

Ambiguity appears also in the choice of the conserved variable. In frames of the barotropic vorticity the only energy that can be conserved is the kinetic one. The shallow water system itself conserves the sum of the kinetic and potential energies. It is, consequently, reasonable to suppose that subgrid scale processes would also keep the total energy, allowing the transfer of kinetic energy to potential one and vice versa. However, it is the spurious kinetic energy loss at small scales that we need to cancel. Potential energy is neither transported toward small scales by the model dynamics, nor undergo spurious dissipation at these scales. Moreover, shallow water is not the final but of our study. We intend to extend this approach to primitive equations full physics models that have more complex energy balance. Instead of analyzing this balance in detail, in this paper we choose to preserve the kinetic energy only.

The purpose of this paper is to use the maximum entropy production principle (MEPP) for the shallow water model and to point out the way to use this principle for primitive equations with both harmonic and biharmonic dissipation.

The paper is organized as follows. In the second section we describe and discuss the shallow water model, define the probability density functions and develop the maximum entropy production principle. In the third section we perform numerical experiments with the model in a square box with a set of different resolution grids and compare results.

2 Model setup

We consider shallow water model in the conventional formulation

$$\begin{aligned}
\frac{\partial u}{\partial t} &= v(\zeta + f) - \frac{\partial B}{\partial x} - bu + D_u + \tau_x \\
\frac{\partial v}{\partial t} &= -u(\zeta + f) - \frac{\partial B}{\partial y} - bv + D_v + \tau_y \\
\frac{\partial h}{\partial t} &= -\frac{\partial hu}{\partial x} - \frac{\partial hv}{\partial y}
\end{aligned} \tag{1}$$

with impermeability and no-slip boundary conditions. In this system u and v denote zonal and meridional velocities, h is the sea surface elevation, $\zeta = \frac{\partial v}{\partial x} -$

$\frac{\partial u}{\partial y}$, $\xi = \frac{\partial u}{\partial x} + \frac{\partial v}{\partial y}$ are relative vorticity and divergence, and $B = \frac{u^2+v^2}{2} + gh$ is the Bernoulli potential. Coriolis parameter f simulates the effect of the Earth rotation, coefficient b parametrizes the bottom drag and τ_x, τ_y is the parametrization of the wind stress applied to the surface of the ocean. D_u and D_v describe the parametrization of the influence of subgrid scales. Conventionally, these terms represent Laplacian dissipation responsible for the enstrophy sink near the grid scales:

$$D_u = A\Delta u,\ D_v = A\Delta v \tag{2}$$

We consider D_u, D_v as a diffusive flux that represents the influence of subgrid scales on the dynamics rather than a simple Newtonian sink of energy and enstrophy. To redefine the terms D_u and D_v we suppose that the relative vorticity ζ and the divergence ξ have a considerable subgrid-scale structure. In other words, we suppose that a probability density functions (PDF) $\rho_{i,j}(\sigma, t)$ and $\chi_{i,j}(\sigma, t)$ can be defined in any grid cell associated with the node i, j . The variable σ has the same dimension $1/s$ as vorticity and divergence. Products $\rho_{i,j}(\sigma, t)d\sigma$ and $\chi_{i,j}(\sigma, t)d\sigma$ show the probability to find vorticity or divergence values in the interval $[\sigma, \sigma + d\sigma]$ in the grid cell i, j.

Both PDF are normalized at each cell

$$\int_{-\infty}^{\infty} \rho_{i,j}(\sigma, t)d\sigma = \int_{-\infty}^{\infty} \chi_{i,j}(\sigma, t)d\sigma = 1 \tag{3}$$

and the cell-mean values of vorticity and divergence are calculated as

$$\zeta_{i,j} = \int_{-\infty}^{\infty} \rho_{i,j}(\sigma, t)\sigma d\sigma, \quad \xi_{i,j} = \int_{-\infty}^{\infty} \chi_{i,j}(\sigma, t)\sigma d\sigma \tag{4}$$

Below, we focus our attention on the diffusive term supposing that this term represents the principal influence of subgrid scales on the flow. We do not take into account advection, forcing and bottom friction terms considering these processes as large scale ones influencing both grid and subgrid scales in the same way. We suppose that no particular subgrid scale effect is produced by these terms.

To obtain the diffusion equations for ρ and χ, we calculate the curl and the divergence of the diffusive part of first two equations of (1) and write equations of diffusion of ζ and ξ

$$\begin{aligned} \frac{\partial \zeta}{\partial t} &= \frac{\partial D_v}{\partial x} - \frac{\partial D_u}{\partial y} \\ \frac{\partial \xi}{\partial t} &= \frac{\partial D_u}{\partial x} + \frac{\partial D_v}{\partial y} \end{aligned} \tag{5}$$

So far, D_u, D_v are considered as a diffusive flux that represents the influence of subgrid scales, we rewrite their formulation in the form that is similar to (4):

$$D_u = \int \mathcal{J}_u \sigma d\sigma, \quad D_v = \int \mathcal{J}_v \sigma d\sigma \tag{6}$$

Combining (5),(6) and (4) we get equations of diffusion of the probability density functions:

$$\begin{aligned}\int \frac{\partial \rho}{\partial t}\sigma d\sigma &= \int\left(\frac{\partial \mathcal{J}_v}{\partial x}-\frac{\partial \mathcal{J}_u}{\partial y}\right)\sigma d\sigma \\ \int \frac{\partial \chi}{\partial t}\sigma d\sigma &= \int\left(\frac{\partial \mathcal{J}_u}{\partial x}+\frac{\partial \mathcal{J}_v}{\partial y}\right)\sigma d\sigma\end{aligned} \tag{7}$$

To develop an explicit form of these fluxes, we impose several requirements. The first and the quite evident requirement is imposed following [7]. It consists in maximizing of entropy production by the subgrid scales. However, accepting that both vorticity and divergence have the subgid scale variability, we get two PDFs ρ and χ and two entropies by these PDFs:

$$S_\rho = -\int\int \rho(\sigma,t)\ln\rho(\sigma,t)d\sigma dxdy,\ S_\chi = -\int\int \chi(\sigma,t)\ln\chi(\sigma,t)d\sigma dxdy \tag{8}$$

It is impossible to maximize both entropies simultaneously. We have a choice either to get the diffusive flux maximizing the sum of them or produce two separate fluxes that maximize S_ρ or S_χ and use the sum of these fluxes. The second way is used in this paper because it is more simple.

The second requirement is imposed to limit the corresponding norm of diffusive flux: $\mathcal{N}_\rho$ when we maximize the production of S_ρ and $\mathcal{N}_\chi$ otherwise.

$$\begin{aligned}\mathcal{N}_\rho &= \int\left(\frac{(\mathcal{J}_u)^2+(\mathcal{J}_v)^2}{2\rho}\right)d\sigma dxdy = const \\ \mathcal{N}_\chi &= \int\left(\frac{(\mathcal{J}_u)^2+(\mathcal{J}_v)^2}{2\chi}\right)d\sigma dxdy = const\end{aligned} \tag{9}$$

As it is discussed in the introduction, the third requirement for both S_ρ or S_χ maximization, aims at avoiding the spurious energy sink. We impose the conservation of the kinetic energy

$$E = \int \frac{u^2+v^2}{2}dxdy = const \tag{10}$$

rather than total energy that is really conserved by the whole system.

This variational problem is treated by introducing Lagrange multipliers A and β (at each time t) so that the condition

$$\delta\mathcal{N} + A\left(\delta\frac{\partial S}{\partial t}+\beta\delta\frac{\partial E}{\partial t}\right) = 0 \tag{11}$$

must be satisfied for any variations $\delta\mathcal{J}$.

The time derivative of the entropy S_ρ writes

$$\begin{aligned}\frac{\partial S_\rho}{\partial t} &= -\int\frac{\partial\rho}{\partial t}(\ln\rho+1)d\sigma dxdy = -\int\left(\frac{\partial \mathcal{J}_v}{\partial x}-\frac{\partial \mathcal{J}_u}{\partial y}\right)(\ln\rho+1)d\sigma dxdy = \\ &= \int\frac{\mathcal{J}_v}{\rho}\frac{\partial\rho}{\partial x}-\frac{\mathcal{J}_u}{\rho}\frac{\partial\rho}{\partial y}d\sigma dxdy\end{aligned} \tag{12}$$

and similarly for S_χ

$$\frac{\partial S_\chi}{\partial t} = \int \frac{\mathcal{J}_u}{\chi}\frac{\partial \chi}{\partial x} + \frac{\mathcal{J}_v}{\chi}\frac{\partial \chi}{\partial y} d\sigma dx dy \tag{13}$$

thanks to integration by parts and to no flux boundary conditions.

Energy derivative can be calculated using (1) and (10) taking into account diffusive terms only

$$\begin{aligned}\frac{\partial E}{\partial t} &= \frac{\partial}{\partial t}\int \frac{u^2+v^2}{2} dxdy = \int \left(u\frac{\partial u}{\partial t} + v\frac{\partial v}{\partial t}\right) dxdy = \\ &= \int (u\mathcal{J}_u + v\mathcal{J}_v)\sigma d\sigma dxdy = 0.\end{aligned} \tag{14}$$

Taking into account (12) and (14), the equality (11) writes for variations of $\mathcal{N}_\rho$ and S_ρ as

$$\begin{aligned}\int \frac{\mathcal{J}_u \delta\mathcal{J}_u + \mathcal{J}_v \delta\mathcal{J}_v}{\rho} d\sigma dx dy &= A\Bigg[\int \left(\frac{\delta\mathcal{J}_v}{\rho}\frac{\partial \rho}{\partial x} - \frac{\delta\mathcal{J}_u}{\rho}\frac{\partial \rho}{\partial y}\right) d\sigma dx dy + \\ &+ \beta \int \left(u\delta\mathcal{J}_u + v\delta\mathcal{J}_v\right)\sigma d\sigma dx dy\Bigg]\end{aligned}$$

and similarly for variations of $\mathcal{N}_\chi$ and of S_χ. Knowing that all $\delta\mathcal{J}$ are independent and non-null, we may consider each variation separately. We get the flux that maximizes the entropy S_ρ

$$\begin{aligned}\frac{\mathcal{J}_u}{\rho} &= -A\left(\frac{1}{\rho}\frac{\partial \rho}{\partial y} + \beta u\sigma + F_1(x,y)\right) \\ \frac{\mathcal{J}_v}{\rho} &= A\left(\frac{1}{\rho}\frac{\partial \rho}{\partial x} + \beta v\sigma + F_2(x,y)\right)\end{aligned}$$

and another flux that maximizes entropy S_χ

$$\begin{aligned}\frac{\mathcal{J}_u}{\chi} &= A\left(\frac{1}{\chi}\frac{\partial \chi}{\partial x} + \beta u\sigma + F_3(x,y)\right) \\ \frac{\mathcal{J}_v}{\chi} &= A\left(\frac{1}{\chi}\frac{\partial \chi}{\partial y} + \beta v\sigma + F_4(x,y)\right)\end{aligned}$$

To determine free terms $F(x,y)$, we multiply each equation either by ρ or by χ and integrate over σ. Taking into account (3), (4) and $\int \mathcal{J} d\sigma = 0$, we get

$$-\beta u\zeta = F_1(x,y),\ -\beta v\zeta = F_2(x,y),\ -\beta u\xi = F_3(x,y),\ -\beta v\xi = F_4(x,y).$$

As it is noted above, the total diffusive flux is defined as the sum of two fluxes that maximize S_ρ and S_χ.

$$\begin{aligned}\mathcal{J}_u &= A\left(\frac{\partial \chi}{\partial x} - \frac{\partial \rho}{\partial y} + \beta u(\chi(\sigma-\xi) + \rho(\sigma-\zeta))\right) \\ \mathcal{J}_v &= A\left(\frac{\partial \chi}{\partial y} + \frac{\partial \rho}{\partial x} + \beta v(\chi(\sigma-\xi) + \rho(\sigma-\zeta))\right)\end{aligned}$$

To calculate the parameter β we use the condition of the energy conservation (14) by the diffusive flux

$$\begin{aligned}\frac{\partial E}{\partial t} &= 0 = \int (u\mathcal{J}_u + v\mathcal{J}_v)\sigma d\sigma dxdy = \\ &= A\int\left(u\frac{\partial \chi}{\partial x} - u\frac{\partial \rho}{\partial y} + v\frac{\partial \chi}{\partial y} + v\frac{\partial \rho}{\partial x} + \beta(u^2+v^2)(\chi(\sigma-\xi)+\rho(\sigma-\zeta))\right)\sigma d\sigma dxdy\end{aligned}$$

Combining all terms with β and integrating in σ we get

$$\int\left(u\frac{\partial \xi}{\partial x} - u\frac{\partial \zeta}{\partial y} + v\frac{\partial \xi}{\partial y} + v\frac{\partial \zeta}{\partial x}\right)dxdy = -\beta\int\left(u^2(q_\chi+q_\rho) + v^2(q_\chi+q_\rho)\right)dxdy$$

where q_χ and q_ρ denote the dispersion of distribution of divergence and vorticity parcels within each grid cell:

$$\begin{aligned}q_\chi &= \int \chi(\sigma-\xi)\sigma d\sigma = \int \chi\sigma^2 d\sigma - \xi\int\chi\sigma d\sigma = \overline{\xi^2} - \xi^2 \\ q_\rho &= \int \rho(\sigma-\zeta)\sigma d\sigma = \overline{\zeta^2} - \zeta^2\end{aligned} \tag{15}$$

where overline denotes an average over a grid cell.

Consequently, the influence of subgrid scales (6) in the model (1) is determined by

$$\begin{aligned}D_u &= \int \mathcal{J}_u\sigma d\sigma = A\left(\frac{\partial \xi}{\partial x} - \frac{\partial \zeta}{\partial y} + \beta u(q_\chi+q_\rho)\right) = A\left(\Delta u + \beta u q\right) \\ D_v &= \int \mathcal{J}_v\sigma d\sigma = A\left(\frac{\partial \xi}{\partial y} + \frac{\partial \zeta}{\partial x} + \beta v(q_\chi+q_\rho)\right) = A\left(\Delta v + \beta v q\right)\end{aligned} \tag{16}$$

where β is defined by

$$\beta = -\frac{\int\left(u(\frac{\partial \xi}{\partial x} - \frac{\partial \zeta}{\partial y}) + v(\frac{\partial \xi}{\partial y} + \frac{\partial \zeta}{\partial x})\right)dxdy}{\int q(u^2+v^2)dxdy} \tag{17}$$

and $q = q_\chi + q_\rho$ (15) contains the second statistical moment and require a closure hypothesis. The simplest one is to suppose that $q = const$ in any grid cell. The value of this constant is not important because it is simplified in (16) and in the denominator of β (17).

Alternative idea consists in the assumption that the dispersion in the cell is proportional to the square of the difference of mean values in the neighboring cells. This implies larger distributions in regions with high gradients of vorticity and divergence.

$$\begin{aligned}q_{i,j} &\sim \left((\zeta_{i+1,j} - \zeta_{i-1,j})^2 + (\zeta_{i,j+1} - \zeta_{i,j-1})^2\right) \\ &+ \left((\xi_{i+1,j} - \xi_{i-1,j})^2 + (\xi_{i,j+1} - \xi_{i,j-1})^2\right)\end{aligned} \tag{18}$$

Despite we require $q_{i,j}$ to be proportional to the square of the difference, we can use one as the proportionality multiplier for the same reason as before: this multiplier will be simplified with the denominator of β.

We can note here, that the hypothesis of constant q implies that the backscattering term is weighted by u and v only. The energy flux from subgrid scales is assumed to be proportional to the grid energy. This reasonable hypothesis, however, may not fit well to simulation of turbulent flows, especially with strong boundary layers and jet streams. In this case, it may be reasonable to use the expression (18) that ensures an additional weighting in regions of high gradients of ζ and ξ, i.e. regions of high dissipation. The injection of energy in this case is increased in jet streams and boundary layers and reduced in regions of laminar flow.

Another hypothesis we can use for finer tuning of the backscattering process consists in adding of a positive constant to $q_{i,j}$ separating its value from zero. Choosing this constant either small or big with respect to vorticity gradient, we can obtain the backscatter energy balance close to the balance defined either by (18) or by the condition $q = const$. Some intermediate value may help us to better balance the energy dissipation and its compensation by backscattering. This tuning, however, is beyond the scope of this paper because we study just the principal properties of this backscattering in frames of a simple shallow water model.

Coefficient β defined by (17) ensures exact compensation of the dissipated energy. This is absolutely necessary when the purpose is to find the statistical equilibrium state of inviscid unforced model as in [8, 16]. Working with forced and dissipative models may require another balance between sink and compensation of the kinetic energy. Having bottom friction (or vertical dissipation) as the only energy sink may modify the energy balance of the model. Thus, in this paper we multiply β by additional coefficient 0.7 and reinject only 70% of dissipated energy in order to avoid emerging of spurious wave regime non observed at high resolution.

3 MEPP test

Proposed method is tested in the square-box model configuration. We consider $30^\circ \times 30^\circ$ box placed in the mid-latitudes region $24^\circ \leq \varphi \leq 54^\circ$. The model is forced by the zonal wind stress

$$\tau_x = -0.18 \frac{N}{m^2} \cos \frac{2\pi(\varphi - 24^\circ)}{30^\circ},\ \tau_y = 0$$

Bottom friction parameter is chosen as $b = 10^{-7} s^{-1}$ and the reduced gravity as $g = 0.02 m/s^2$. Beta-plane approximation is used for the Coriolis parameter

$$f = 6 \times 10^{-5} \left(1 + \frac{(\varphi - 24^\circ)}{30^\circ}\right) s^{-1}$$

Experiments are carried out on the set of four grids with different spatial resolutions varying from 0.6° to 0.075°. The coarsest grid counts 50×50 nodes and the finest one — 400×400. The same coefficient A was used in the conventional diffusion (2) and in the MEPP parametrisation of subgrid scales (16). This coefficient was, however, adapted to the resolution: lower value is used for finer resolution starting at $A = 480\frac{m^2}{s}$ for the resolution 0.6° down to $A = 60\frac{m^2}{s}$ at the finest resolution. At each resolution in these tests we compare the model solutions with different parametrizaitions of subgrid scale effects. Results obtained using classical Laplacian dissipation (2) and MEPP parametrization (16) are compared with each other.

In each experiment and for each subgrid scales parametrization we perform a spin-up of the model during 10 years. After that, 50 years model run is analyzed and averages over this period are discussed.

The model solution at the finest grid will be used below as the reference one. The grid is composed of 400×400 nodes provides the 0.075° resolution of the 30° × 30° square. Only conventional Laplacian (2) dissipation is used in this experiment with the lowest possible coefficient $A = 60\frac{m^2}{s}$. We consider averaged sea surface height and eddy kinetic energy shown in fig.1.

$$\mathcal{E} = \frac{1}{2}\left[\int_{10yr}^{60yr} u^2 + v^2 dt - \left(\int_{10yr}^{60yr} u dt\right)^2 - \left(\int_{10yr}^{60yr} v dt\right)^2\right] \tag{19}$$

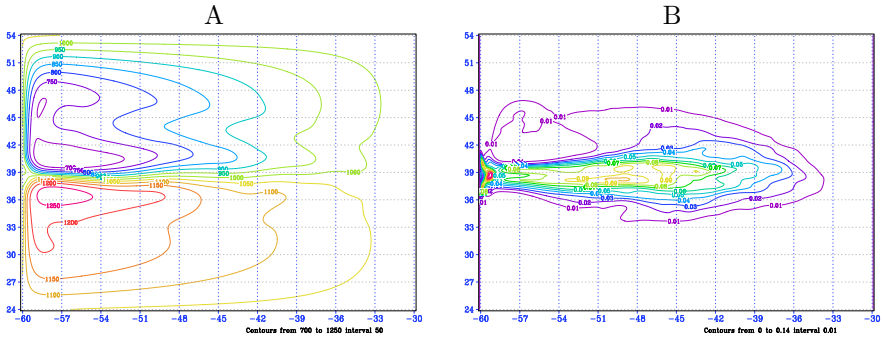

Figure 1: 50 years mean sea surface height (A) and eddy kinetic energy (B) in the experiment with 0.075° resolution.

The flow is characterized by the strong western boundary currents with formation of the jet flux near the center of the square. Velocity of the flow near the western wall and in the jet exceeds 1 m/s. The jet is characterized by the strong and unstable meandering that defines the major part of the variability of the flow. However, the maximum of eddy kinetic energy (fig.1B) is situated near the western boundary showing the impact of the variation of the point of jet stream separation from the wall.

Experiments on the grid with two times coarser resolution (200×200 nodes with $0.15°$ resolution) show a quite similar flow configuration with slightly lower variability (fig.2). Eddy kinetic energy lost 1/3 of its former value both in the meandering region and at the maximum point near the western boundary. We can also note that the jet stream is amplified in the Western half of the square (to the west from the $-45°$ longitude) and reduced in the Eastern half. Eddy kinetic energy pattern shows also insufficient variability to the East from $-39°$ longitude.

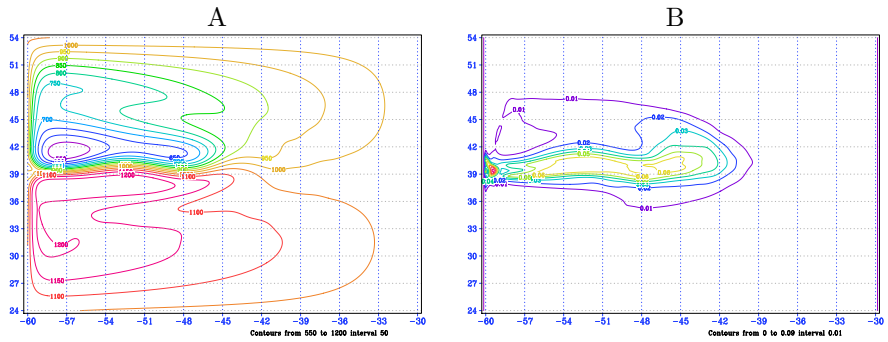

Figure 2: Average sea surface height (A) and eddy kinetic energy (B) in the experiment with $0.15°$ resolution and conventional viscosity.

Of course, this is explained by lower resolution and higher dissipation coefficient $A = 120\frac{m^2}{s}$ that is necessary to avoid numerical noise. In order to compensate excessive sink of the kinetic energy (and particularly eddy kinetic energy) we use the MEPP principle and add the backscattering term (16) with the weight β defined by (17) assuming here that q in these equations is a constant for any grid cell.

Indeed, adding the backscattering term results in a more energetic flow. Eddy energy in fig.3 considerably increases exceeding not only the energy obtained with the conventional viscosity but also the reference experiment with double resolution. The SSH pattern also shows an amplified dipole. However, only the highest point of the sea surface becomes higher rather than the length of the jet.

In order to make the geographical distribution of EKE closer to the reference one and increase the length of the jet, we apply more sophisticated backscattering allowing the second statistical moment to vary from one grid cell to another. As it has been noted, we use the approximation (18) assuming that dispersions of χ and ρ must be bigger in regions with big gradients of ξ and ζ.

Sea surface height and eddy kinetic energy obtained in the experiment with this parametrization are shown in fig.4. One can see both shapes and values in this figure are closer to the reference experiment shown in fig.1.

If we reduce the resolution once more, passing to 100×100 nodes with $0.3°$ resolution, then using conventional diffusion would result in a similar SSH

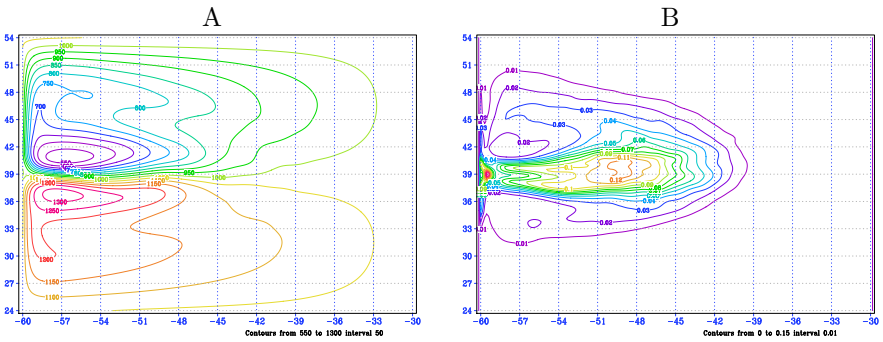

Figure 3: Average sea surface height (A) and eddy kinetic energy (B) in the experiment with 0.15° resolution and MEPP viscosity with constant q.

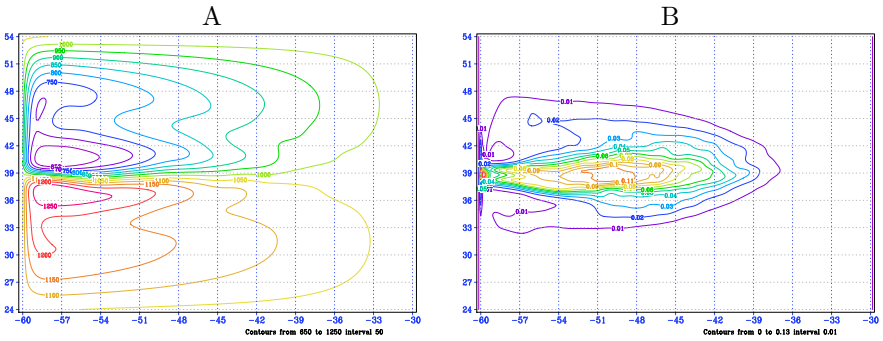

Figure 4: Average sea surface height (A) and eddy kinetic energy (B) in the experiment with 0.15° resolution and MEPP viscosity with variable q estimated according to (18).

shape with drastically reduced variability shown in fig.5. Eddy kinetic energy completely lost the maximum near the boundary and only a little variability remained in the jet area.

Using MEPP viscosity with variable dispersion q allows us to bring the low-resolution flow closer to the simulation obtained at high resolution. The gradient of SSH is overestimated and the length of the jet is smaller than in the reference experiment, but the EKE shows developed variability in the jet region and reappeared maximum near the western boundary at the point of jet stream separation from the wall.

At the resolution 0.6° the solution is stationary with any subgrid scales parametrization. Using MEPP approach helps to increase the length of the jet in the middle of the square box (see fig.7). We can note that using constant q provides a longer jet stream than with the variable q. However, comparing the jet length with higher resolution experiments shown above, we note that

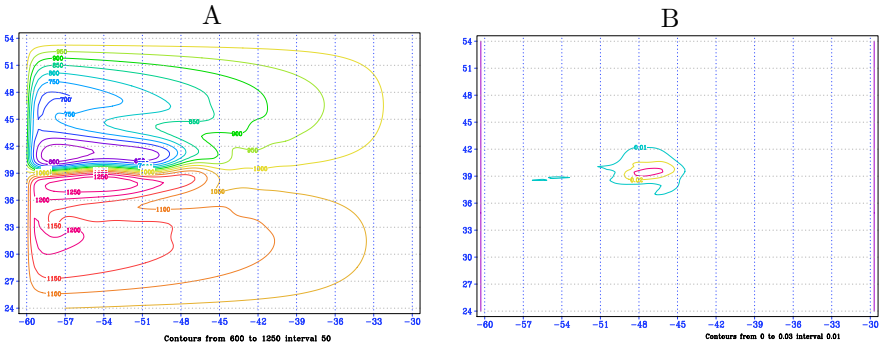

Figure 5: Average sea surface height (A) and eddy kinetic energy (B) in the experiment with 0.3° resolution and conventional viscosity.

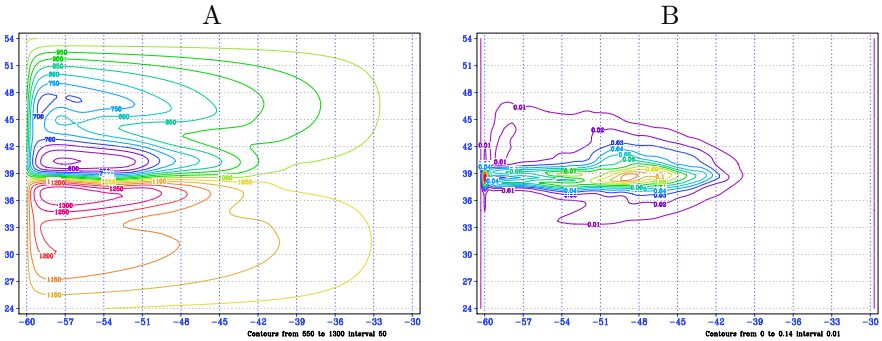

Figure 6: Average sea surface height (A) and eddy kinetic energy (B) in the experiment with 0.3° resolution and MEPP viscosity with variable q estimated according to (18)..

the length is better approximated using backscattering with variable q obtained according to (18). The SSH shape obtained with the constant q overestimates also the maximum and minimum sea surface height.

On the other hand, no variability is added to the flow by MEPP parametrization and the flow remains stationary. The resolution is too coarse to allow any variability.

Consequently, we see that MEPP backscattering can improve the model solution and bring a low resolution flow closer to the high resolution one. However, there exists a limit grid resolution, apparently situated between 0.3° and 0.6°, that makes the backscattering less useful. This limit resolution is, in fact, a well known Rossby deformation radius $R = \sqrt{gH}/f$ that is here equal to $50km$ for parameters given above. It is well known that a shallow water model on the C-grid cannot correctly represent the gravitational waves and suffers from grid-

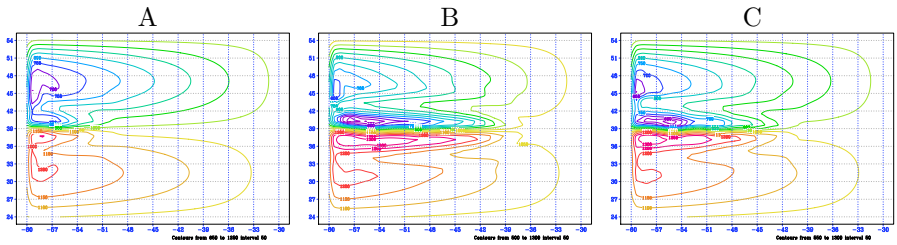

Figure 7: Stationary sea surface height in the experiment with resolution 0.6°. Conventional dissipation (A), MEPP parametrization with constant (B) and with variable (18) q (C).

scale noise when the resolution is lower that the Rossby radius. This property can be traced back to the spatial averaging of the Coriolis terms on the C-grid [17, 18].

In order to analyze the balance of energy by the dissipation and backscattering terms, we write the equation for the evolution of the kinetic energy (10) writing the sum of the first two equation multiplied by u and v respectively

$$\frac{\partial E}{\partial t} = \frac{1}{2}\int\left(-u\frac{\partial B}{\partial x} - v\frac{\partial B}{\partial y} - b(u^2+v^2) + \tau_x u + \tau_y v + uD_u + vD_v\right)dxdy$$

So far, we are interested in the sources and sinks of the kinetic energy provided by subgrid scales, we consider only two terms containing D_u and D_v. Substituting their explicit form (16), we get

$$\begin{aligned}
\frac{\partial E_{subgrid}}{\partial t} &= \frac{1}{2}\int\left(uD_u + vD_v\right)dxdy = \\
&= \frac{A}{2}\int\left(u\Delta u + v\Delta v + \beta q(u^2+v^2)\right)dxdy = \\
&= -\frac{A}{2}\int\left[\left(\frac{\partial u}{\partial x}\right)^2 + \left(\frac{\partial u}{\partial y}\right)^2 + \left(\frac{\partial v}{\partial x}\right)^2 + \left(\frac{\partial v}{\partial y}\right)^2\right]dxdy + \quad (20)\\
&+ \quad \frac{A}{2}\int \beta q(u^2+v^2)dxdy \quad (21)
\end{aligned}$$

thanks to integration by parts and impermeability boundary conditions. Expression (20) shows the dissipation of energy due to the first term of the subgrid scale influence and (21) — the compensation of energy due to backscattering.

To see the regional distribution of the energy sources and sinks, we plot the 50 years mean expressions under integral in (20) and (21). However, the value of these terms show significant spatial variance, dissipation and backscattering in turbulent regions is 10^6 times bigger than in regions where flow is laminar. To better see this wide range in the same picture, we plot the decimal logarithm of these expressions.

One can see in fig.8A that in the reference experiment the highest dissipation occurs in the western boundary layer where its value reaches $2.7 \times 10^{-6} m^2/s^3$. In the jet area we see 1 to 2 orders lower dissipation while outside the jet the laminar flow dissipates $10^{-11} \dots 10^{-12} m^2/s^3$ only. Moreover, the dissipation of energy is approximately of the same order for both resolutions. Comparing the dissipation of the reference model in fig.8A with the model on the 0.3° grid shown in fig.8B, we see that in the jet area and outside the jet, the dissipation of the coarse resolution model is just 3 or 5 times higher. This can be explained by the dissipation coefficient which is also 4 times bigger at the coarse resolution. The only exception is observed in the Western boundary layer where the fine grid model shows triple dissipation of energy thanks to finer approximation of the boundary current.

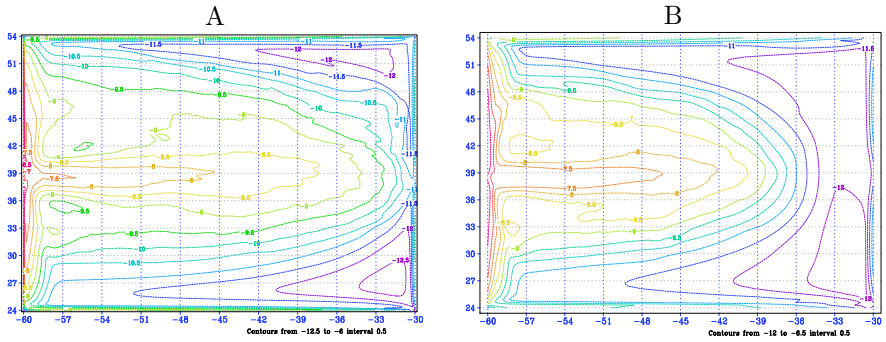

Figure 8: Decimal logarithm of the dissipation of energy in experiments with 0.075° (A) and 0.3° (B) resolutions.

Analyzing the compensative part of the energy balance (21), we compare the backscattering term with constant and variable approximations of the dispersion q obtained by the model on the 0.3° grid. These pictures are shown in fig.9.

As it has been already mentioned, the energy backscattering with constant q is more uniform than with the variable one. In the laminar flow area (on the East), the dissipated energy is reinjected at rate $10^{-11} m^2/s^3$ while in the Western boundary current and in the jet the backscattering reaches $8 \times 10^{-8} m^2/s^3$.

The backscattering obtained using variable q shows more variance. In the Eastern part of the square the backscattering is negligible with respect to the dissipation and the rate of energy injection in the boundary layer is $8 \times 10^{-7} m^2/s^3$. That means the backscattering compensate the major part of the energy loss near the boundary and in the jet stream without influencing the dissipation in the laminar flow regions.

We can note here that variable q approximation results in the negative energy balance everywhere in the square box. Backscattering of energy is always lower than its dissipation. In the laminar flow regions, the dissipation is 100 – 500 times bigger than the compensation and in the region with considerable vorticity (jet area and boundary layer) the compensation values either reach parity with

the dissipation or remain 3-5 times lower.

Approximation $q = const$ results in the domination of backscattering in front of dissipation in laminar flow regions where the energy injection can be 30 times higher than the dissipation. In the same time, the dissipation dominates 10 times the injection in the boundary layer. We can say that the energy is pumped out from the turbulence and reinjected in large-scale laminar flow. This property helps to achieve the statistical equilibrium state in an unforced inviscid fluid which is the goal of this approach formulated in [16, 8]. However, using this method to parametrize the subgrid scale influence to a more realistic flow without aiming at equilibrium state, we should better introduce a local approximation of the PDF dispersions in a grid cell like (18) to be capable to manage the energy balance in a turbulent flow.

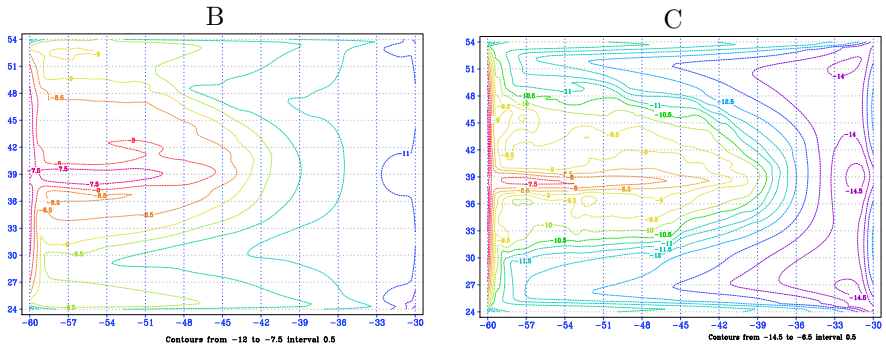

Figure 9: Decimal logarithm of the backscattering with constant (A) and variable (B) q. Experiment with resolution 0.3°.

Another interesting method of study of the model behavior and its comparison with observational data consists in the analysis of the fields variance on different spatial scales. Fourier decomposition and spectral analysis allows us to understand different flow regimes over different wavelength ranges. Thus, the separation of long scales and mesoscales can clearly be distinguished in the kinetic energy spectra of atmospheric models and observational data (see [19], for example), the deviation of the model spectrum from the expected one has used as a basis of the definition of effective resolution in [20].

In this paper, we also compare kinetic energy spectra produced by the low resolution model with conventional and MEPP parametrizations of subgrid scales and the spectrum of the high resolution reference model. Following [20], we consider the inner part of the basin excluding boundary layers to calculate the kinetic energy spectra. The idea of removing linear trends along all points of constant latitude proposed in [21] is used to calculate spectra in non-periodic domains and for non-periodic data.

Snapshots of the kinetic energy are calculated every 3 months during 50 years model run. Thus, 200 fields have been used to produce Fourier spectra along the longitude. We skip 1.5° distance near each boundary and remove linear

trend from obtained data. Averages of these spectra over all latitudes and all snapshots are presented in fig.10 for three model runs: reference run with conventional viscosity and two runs on the 0.3° resolution grid with conventional and MEPP parametrizations of subgrid scales. MEPP parametrization used approximation of variable $q_{i,j}$ (18).

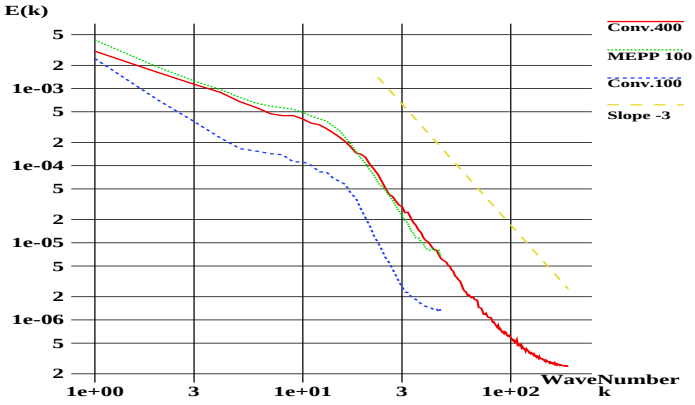

Figure 10: Kinetic energy spectra of the reference model (400×400 grid, solid line) and the model at 0.3° resolution (100×100 grid) with conventional (long dashes) and MEPP (short dashes) parametrizations of subgrid scales.

Of course, in frames of a shallow water model we can not distinguish the region with $-5/3$ slope that is observed in full physics atmospheric models and observational data. All lines in fig.10 contain four parts with different slopes and neither of them can be approximated by $-5/3$. In the long waves limit, the spectrum behaves as k^{-1} or $k^{-1.5}$. After that, in the region $5 < k < 15$, there is a significant shallowing of the slope indicating the concentration of energy in waves from 200 to 600 km length. We observe well known k^{-3} slope that characterizes classical two-dimensional turbulence at shorter waves with a slight decreasing of the slope at higher wavenumbers. This deviation from the canonical k^{-3} law has been explained in [22] by the influence of the inertia-gravity wave component that become comparable with the potential-vortical one.

Analyzing fig.10, we note that conventional viscosity at low resolution reduces energy part of all wavenumbers. The energy that correspond to long waves is 5 times lower than in the reference model. The difference increases with the wavenumber reaching 10.

MEPP backscattering compensates the loss of energy over range of wavenumbers and brings the low resolution model spectrum close to the high resolution one.

4 Conclusion

We have analyzed the influence of the MEPP parametrization of subgrid scale processes and have proposed an explicit formulation of the corresponding backscattering term. Several experiments carried out with the shallow water model in a square box show the possibility to compensate the spurious energy sink by the classical dissipation operator. Two forms of the compensation operator have been constructed and tested. It has been shown that using backscattering with variable q approximation according to (18) allows the model to get better spatial distribution of the energy flux while the approximation $q = const$ pump the energy out in turbulent regions reinjecting it to the laminar flow.

Numerical experiments show that the proposed parametrization allows us to reduce 4 times the resolution and to obtain the flow which is quite similar to the reference model. Comparing figures with the time mean sea surface height, time mean eddy kinetic energy (see fig.1 and fig.6) and kinetic energy spectrum (see fig.10) we find that MEPP parametrization is able to reproduce the principal features of the high resolution reference model while requiring approximately 50 times less computer time. It allows to run the model on the grid containing 16 times less nodes with 4 times longer time step requiring four additional loops ((16), (17) and (18)) over the whole domain for both u and v velocity components. There is, however, a natural resolution limit: Rossby deformation radius must be explicitly resolved by the grid. Otherwise, the model dynamics is poorly approximated and no backscattering can improve the situation.

Theoretical development and numerical experiments in frames of shallow water model can be considered as a first step toward the real implementation of this backscattering in a three dimensional ocean general circulation model. Such an implementation would require finer tuning and numerical tests. However, proposed MEPP parametrization allows us to perform such a tuning. As it has been noted above, we can add a positive constant to $q_{i,j}$ (18) to separate its value from zero in cases when this helps to improve spatial distribution of the backscattering energy flux.

Taking into account that primitive equations models frequently include biharmonic friction, it may be necessary to reformulate the MEPP parametrization. This can be done by modifying the principal hypothesis of this paper: vorticity and divergence may have a fine structure and considerable variations within grid cells. This hypothesis should be replaced by "Laplacian of u and v may have a fine structure while vorticity and divergence become supposed to be smooth as well as velocities. Under such assumption, parametrization of subgrid scales will be represented by bilaplacian that manages the enstrophy dissipation and corresponding backscattering to compensate the loss of kinetic energy.

Basing on the maximum entropy production principle, we constructed the parametrization of the influence of subgrid scales and tested it on the shallow water model in a square box. Experiment shown the ability of this parametrization to bring the model solution toward the solution of the same model on the finer grid. Both mean fields and variability of the model on a coarse grid become

closer to the behavior on a fine grid. This fact indicates the interest to continue the study in frames of full physics three-dimensional ocean model.

References

[1] Boussinesq J. Essai sur la théorie des eaux courantes. *Mémoires présentés par divers savants l'Académie des Sciences* 1877; **23**(1):1–680.

[2] Reynolds O. On the dynamical theory of incompressible viscous fluids and the determination of the criterion. *Phil. Trans. R. Soc. London* 1895; **186**:123–164.

[3] Charney JG. Geostrophic turbulence. *Journal of the Atmospheric Sciences* 1971; **28**(6):1087–1095.

[4] Kraichnan RH. Eddy viscosity in two and three dimensions. *Journal of the Atmospheric Sciences* 1976; **33**(8):1521–1536.

[5] Leith CE. Stochastic backscatter in a subgridscale model: Plane shear mixing layer. *Phys. Fluids A 2* 1990; **297**:297–299.

[6] Shutts G. A kinetic energy backscatter algorithm for use in ensemble prediction systems. *Quarterly Journal of the Royal Meteorological Society* 2005; **131**(612):3079–3102, doi:10.1256/qj.04.106.

[7] Kazantsev E, Sommeria J, Verron J. Subgrid-scale eddy parameterization by statistical mechanics in a barotropic ocean model. *Journal of Physical Oceanography* 1998; **28**(6):1017–1042.

[8] Chavanis PH, Sommeria J. Statistical mechanics of the shallow water system. *Physical Review E : Statistical, Nonlinear, and Soft Matter Physics* 2002; **65**(2):026 302.

[9] Polyakov I. An eddy parameterization based on maximum entropy production with application to modeling of the arctic ocean circulation. *Journal of Physical Oceanography* 2001; **31**(8):2255–2270.

[10] Nadiga BT, Bouchet F. The equivalence of the lagrangian-averaged Navier-Stokes-α model and the rational large eddy simulation model in two dimensions. *Physics of Fluids* 2011; **23**(9):095–105.

[11] Nadiga BT, Shkoller S. Enhancement of the inverse-cascade of energy in the two-dimensional lagrangian-averaged Navier–Stokes equations. *Physics of Fluids* 2001; **13**(5):1528–1531.

[12] Holm DD, Nadiga BT. Modeling mesoscale turbulence in the barotropic double-gyre circulation. *Journal of physical oceanography* 2003; **33**(11):2355–2365.

[13] Graham JP, Ringler T. A framework for the evaluation of turbulence closures used in mesoscale ocean large-eddy simulations. *Ocean Modelling* 2013; **65**:25 – 39, doi:http://dx.doi.org/10.1016/j.ocemod.2013.01.004.

[14] Jansen MF, Held IM. Parameterizing subgrid-scale eddy effects using energetically consistent backscatter. *Ocean Modelling* 2014; **80**:36 – 48, doi: http://dx.doi.org/10.1016/j.ocemod.2014.06.002.

[15] Jansen MF, Held IM, Adcroft A, Hallberg R. Energy budget-based backscatter in an eddy permitting primitive equation model. *Ocean Modelling* 2015; **94**:15 – 26, doi: http://dx.doi.org/10.1016/j.ocemod.2015.07.015.

[16] Robert R, Sommeria J. Relaxation towards a statistical equilibrium state in two-dimensional perfect fluid dynamics. *Phys. Rev. Lett.* Nov 1992; **69**:2776–2779.

[17] Arakawa A, Lamb V. Computational design of the basic dynamical processes of the ucla general circulation model. *Methods in Computational Physics* 1977; **17**:174–267.

[18] Fox-Rabinovitz MS. Computational dispersion of horizontal staggered grids for atmospheric and ocean models. *MWR* 1991; **119**:16241639.

[19] Nastrom GD, Gage KS. A climatology of atmospheric wavenumber spectra of wind and temperature observed by commercial aircraft. *Journal of the Atmospheric Sciences* 1985; **42**(9):950–960.

[20] Skamarock WC. Evaluating mesoscale NWP models using kinetic energy spectra. *Monthly Weather Review* 2004; **132**(12):3019–3032, doi: 10.1175/MWR2830.1.

[21] Errico RM. Spectra computed from a limited area grid. *Monthly Weather Review* 1985; **113**(9):1554–1562.

[22] Yuan L, Hamilton K. Equilibrium dynamics in a forced-dissipative f-plane shallow-water system. *Journal of Fluid Mechanics* 12 1994; **280**:369–394, doi:10.1017/S0022112094002971.